WARSAW UNIVERSITY OF TECHNOLOGY

ENGINEERING AND TECHNOLOGY

MATERIALS ENGINEERING

Ph.D. Thesis

Damian Sobieraj, M.Sc.

Phase stability and short-range ordering of W-based SMART materials and high-entropy alloys predicted from the first-principles modelling

Supervisor

dr hab. inż. Jan S. Wróbel

WARSAW

Thanks.

This work was funded by the following projects:

HOMING project nr. Homing/2016-1/12 granted by Foundation for Polish Science, titled:
„Ab initio modeling of phase stability and properties of high entropy alloys"
"Modelowanie ab-initio stabilności fazowej i właściwości stopów o wysokiej entropii"

"Implementation of activities described in the Roadmap to Fusion during Horizon 2020
through a Joint programme of the members of the EUROfusion consortium"
Grant agreement no 633053. Horizon 2020

„Ewolucja mikrostruktury w stopach o wysokiej entropii Ta-Ti-V-W: od symulacji ab initio
do technologii druku 3D", UMO-2019/35/D/ST5/03526, SONATA-15,
National Science Centre

Abstract

A comprehensive study has been carried out on the phase stability and short-range ordering of W-based High-Entropy Alloys (HEAs) in the W-Cr-Ta-Ti-V system, and Self-passivating Metal Alloys with Reduced Thermo-oxidation (SMART) in the W-Cr-Y-Zr system, as potential candidates for application in the future fusion power plants. By applying first-principles thermodynamic study, including Density Functional Theory (DFT), Cluster Expansion (CE) method and Monte Carlo (MC) simulations for temperature-dependent properties, the research offers detailed insights into the formation and stability of various alloy phases.

The study allows to understand how different atomic combinations and their compositions influence the formation of solid solutions and ordered structures in two groups of W-based alloys. Through the detailed analysis of the Short-range Order Parameter (SRO), it is shown that in HEAs from the W-Cr-Ta-Ti-V system, the strongest attraction occurs between Cr and V, as well as Ta and W atoms. The lowest order-disorder transition temperature (ODTT), therefore the widest range of temperatures at which disordered solid solution is present, has been observed for the quaternary W-Ta-Ti-V alloy. Additionally, the model developed in this study has been used to explain the mechanisms behind the formation of experimentally observed Cr and V-rich precipitates in the W38-Ta36-Cr15-V11 alloy with high radiation resistance.

Calculations performed for SMART materials in the W-Cr-Y-Zr system revealed that the addition of Zr in small concentrations stabilizes Y precipitates and helps maintain an optimal order-disorder transition temperature for potential applications.

The following study contributes to the theoretical understanding of complex alloys while also setting a foundation for future experimental validations and the potential for industrial applications of W-based HEAs and SMART materials. Through the theoretical approach, the research highlights the importance of atomic-level interactions determining the material properties and opens new avenues for the design and optimization of advanced metallic alloys.

Keywords: phase stability, high entropy alloy, self-passivating alloys, *ab initio*, Monte Carlo simulations

Streszczenie

W ramach niniejszej pracy wykonano badania nad stabilnością fazową i uporządkowaniem bliskiego zasięgu stopów o wysokiej entropii (HEAs - z ang. High-Entropy Alloys) z układu W-Cr-Ta-Ti-V, oraz samopasywujących się materiałów (SMART - z ang. Self-passivating Metal Alloys with Reduced Thermo-oxidation) z układu W-Cr-Y-Zr, będących potencjalnymi kandydatami do zastosowań w reaktorach syntezy termojądrowej. W celu zrozumienia mechanizmów termodynamicznych i strukturalnych występujących w badanych stopach wykorzystano modelowanie oparte na Teorii Funkcjonału Gęstości (DFT – z ang. Density Functional Theory), metodzie Rozwinięcia Klastrowego (CE – z ang. Cluster Expansion) i symulacjach Monte Carlo (MC)

Przeprowadzone symulacje pozwoliły zrozumieć, w jaki sposób różne pierwiastki i ich stężenia wpływają na tworzenie się roztworów stałych i struktur uporządkowanych w dwóch grupach stopów na bazie W. Poprzez szczegółową analizę parametrów uporządkowania bliskiego zasięgu wykazano, iż w stopach o wysokiej entropii z układu W-Cr-Ta-Ti-V najsilniejsze przyciąganie występuje pomiędzy atomami Cr i V, oraz Ta i W. Najniższą temperaturę przemiany porządek-nieporządek, a zatem najszerszy zakres temperatur występowania roztworu stałego, posiadał czteroskładnikowy stop W-Ta-Ti-V. Model stworzony w ramach niniejszej pracy pozwolił także na wyjaśnienie mechanizmów powstawania eksperymentalnie zaobserwowanych wydzieleń bogatych w Cr i V w stopie W38-Ta36-Cr15-V11 o wysokiej odporności na promieniowanie.

Obliczenia wykonane dla materiałów SMART wykazały, iż dodanie Zr w małych stężeniach stabilizuje wydzielenia Y w stopach z układu W-Cr-Y-Zr, jednocześnie pozwalając na osiągnięcie optymalnej, z punktu widzenia potencjalnych zastosowań, temperatury przemiany porządek-nieporządek.

Uzyskane wyniki przyczyniają się do lepszego teoretycznego zrozumienia wieloskładnikowych stopów, jednocześnie stanowiąc fundament pod przyszłe walidacje eksperymentalne i potencjalne zastosowania materiałów SMART i HEAs na bazie W. Przeprowadzone symulacje podkreślają znaczenie interakcji na poziomie atomowym w kształtowaniu właściwości materiałów i otwierają nowe drogi do projektowania i optymalizacji zaawansowanych stopów metalicznych

Słowa kluczowe: stabilność fazowa, stopy o wysokiej entropii, stopy samopasywujące, *ab initio,* symulacje Monte Carlo

Table of Contents

1 Introduction

The quest for clean and sustainable energy has directed scientific research towards the development of fusion power plants, a promising horizon in the energy landscape. It offers the perspective of abundant energy with minimal environmental impact. However, the realization of viable fusion power plants relies heavily on advancements in materials science, particularly in the development of materials capable of withstanding the extreme conditions within a fusion reactor itself.

Tungsten (W), with its high melting point and substantial mechanical strength at elevated temperatures, has emerged as a leading candidate for key components within fusion reactors, notably in the divertor, where plasma-facing materials are subjected to intense thermal and neutron flux. Despite its desirable properties, pure tungsten has several drawbacks, including brittleness at lower temperatures and a susceptibility to radiation damage, which can severely limit its longevity and performance in a fusion environment - both during regular operation and in case of accidents.

The exploration of W-based Self-passivating Metal Alloys with Reduced Thermo-oxidation (SMART) materials and high-entropy alloys (HEAs) aligns with challenges introduced with future fusion power plants, namely the development of materials with enhanced mechanical properties, radiation resistance, and thermal stability. SMART materials, with their ability to autonomously respond to environmental changes, offer innovative solutions to issues like Loss Of Coolant Accidents (LOCA), where rapid material response could mitigate potential damage. Meanwhile, HEAs, characterized by their complex, multi-principal element compositions, offer high mechanical strength, ductility, and resistance to radiation-induced degradation, addressing key vulnerabilities of pure tungsten.

.

2 Scope of the research, objectives and hypothesis

The goal of this study is to predict the thermodynamic and structural properties of multicomponent high-entropy alloys and SMART materials, for a potential application in future fusion power plants. Since experimental research on endless possible atomic configurations and concentrations in multicomponent materials is impossible, a theoretical approach has been applied. To reach the goal of this work, a number of objectives has been set:

- Creation of the initial structures database for binary, ternary, quaternary and quinary structures in W-based W-Cr-Ta-Ti-V and W-Cr-Y-Zr systems
- Calculation of the enthalpies of mixing and formation energies of all structures at absolute zero, using DFT methods
- Creation of a CE DFT-based model for both, HEAs and SMART materials, with further expansion of the initial database
- Simulating, with the use of MC methods, atomic structures with different atomic compositions and concentrations at finite temperatures
- Analysis of the obtained results, including enthalpies of mixing, formation energies, entropies of mixing, free energies of mixing, order-disorder transition temperatures, short-range order parameters
- Validating obtained results by comparing with already published experimental studies

Therefore, the hypothesis of this thesis is following: phase stability and short-range ordering of W-based high-entropy alloys in W-Cr-Ta-Ti-V system and SMART materials in W-Cr-Y-Zr system can be systematically predicted and optimized through first-principles modeling, by combining Density Functional Theory (DFT), Cluster Expansion (CE) method and Monte Carlo (MC) simulations.

3 Computational methodology

Due to the numerous combinations of element concentrations in various multi-component systems, experimental verification is often time consuming and resource intensive. The increasing capabilities of computers enable their broader application in the field, including the use of modeling methods to reduce the need for experimental research. These methods also provide an opportunity for a more in-depth interpretation of experimental results.

Quantum mechanics-based *ab-initio* methods allow for simulating the atomic structure of various combinations of multiple elements forming crystalline phases. They also enable a quantitative estimation of the properties of the resulting phases, including their enthalpies of mixing, elastic constants, specific heat, and coefficient of thermal expansion. The key advantage of these methods is that they do not require any input data, as existing experimental data is only needed to verify the chosen model.

At the core, the ab-initio methods are based on the numerical solution of the stationary Schrödinger's equation:

$$\widehat{H}\Psi = E\Psi, \tag{3.1}$$

where E is the total energy of the system, Ψ is the wave function of the molecule or the crystal and $\widehat{H}$ is the full Hamiltonian for the multi-atomic system, expressed by including the kinetic energy of the electrons, kinetic energy of the nuclei, electrostatic interaction between the electrons, electrostatic interaction between the nuclei and the electrostatic interaction between the nuclei and electrons.

Unfortunately, because precise numerical and analytical solution of the Schrödinger's equation is only possible for simple structures such as single hydrogen (H) atom, it is necessary to apply numerous approximations to solve it for more complex structures.

According to the Born-Oppenheimer adiabatic approximation, the considerable difference in mass between electrons and ions, with the electron mass to ion mass ratio typically being on the order of 10^4, results in significantly shorter relaxation times for electrons compared to ions. As a consequence, the wave function Ψ can be effectively divided into two distinct subsystems: one comprising of ions and one of electrons. When describing the electron subsystem the ions are considered as static due to their comparatively slower dynamics. Above results in the Hamiltonian being represented by the three terms: kinetic energy $\hat{T}$, internal potential energy $\hat{V}_i$ and external potential energy $\hat{V}_e$:

$$\hat{H} = \hat{T} + \hat{V}_i + \hat{V}_e \tag{3.2}$$

3.1 Density Functional Theory

The fundamental role of the electron density $n(r)$ in the electron ground-state was first formulated by Hohenberg and Kohn in 1964 in the form of two theorems.

The first Hohenberg-Kohn theorem asserts that the ground-state energy of a system built of many electrons, subject to an external potential $v_\alpha(r)$, is a unique functional of the electron density $n(r)$ and can be expressed as:

$$E[n(r)] = \int n(r)v_\alpha(r)dx + F[n(r)],$$

where $F[n]$ is a unique, universal and unknown functional $n(r)$, that is not dependent on the external potential $v_\alpha(r)$. The functional state of the $F[n]$ includes the kinetic, Coulomb and exchange and correlation energies. Since the choice of $v_\alpha(r)$ determines the Hamiltonian function $\hat{H}$, the many-body ground state energy E is a unique functional of $n(r)$. This implies that there is a one-to-one correspondence between the external potential and the electronic density of the ground state.

The second (variational) Hohenberg-Kohn theorem states that the minimum value of the total energy functional $E[n(r)]$, corresponds to the energy of the ground state of the system for the exact electron density $n(r)$ of the ground state, under the condition that the total number of electrons in the system is preserved.

In the following year, Kohn and Sham developed a method that enables the calculation of the kinetic energy of interacting electrons by computing the kinetic energy of a system of non-interacting electrons. They proposed the separation of the universal functional $G[n(r)]$, which includes solely the kinetic and exchange and correlation energies, into two parts:

$$G[n] = T_s[n] + E_{xc}[n],$$

where $T_s[n]$ is the kinetic energy of a system containing non-interacting atoms and $E_{xc}[n]$ is the exchange and correlation functional. Since the second term in (3.4) includes part of the kinetic energy of the system containing interacting atoms, the total energy of the interacting atoms system can be described as:

$$E[n] = \int v_\alpha(r)n(r)dr + \frac{1}{2}\int \frac{n(r)n(r')}{|r-r'|}drdr' + T_s[n] + E_{xc}[n]$$

Density Functional Theory (DFT) computations were executed by employing the Vienna Ab-initio Simulation Package (VASP) software and the Projector Augmented Wave (PAW) technique. The treatment of exchange and correlation functionals followed the Generalized Gradient Approximation by Perdew, Burke and Ernzerhof (GGA-PBE). To make the DFT computations more efficient, PAW potentials lacking semi-core *p* electron contributions were employed for Cr, Ta, Ti, V, W, and Zr, while potentials incorporating semi-core *p* electron contributions were utilized for Y. Notably, the outcomes of DFT computations for the former elements displayed negligible disparities with or without semi-core *p* electron contributions. The investigation did not include magnetism due to the minimal distinction in enthalpies of mixing between anti-ferromagnetic and non-magnetic Cr-rich structures.

Total energies were assessed using the Monkhorst-Pack mesh of *k* points within the Brillouin zone, maintaining a *k*-mesh spacing of 0.2 A, equivalent to a 14x14x14 *k*-point mesh for a two-atom bcc cubic structure. Following preliminary analysis, the plane-wave cutoff energy was established at 400 eV for the calculations. The convergence criterion for the total energy was set at 10^{-6} eV/cell, and the relaxation of force components was executed at a tolerance of 10^{-3} eV/A.

Since the Gibbs free energy at 0 K is equal to zero, the phase stability at 0 K can be described solely by the enthalpy of mixing of a system:

$$\Delta H_{mix}^{bcc}(\vec{\sigma}) = E_{tot}^{bcc}(\vec{\sigma}) - \sum_{p=1}^{K} c_p E_{tot}^{bcc}(p), \tag{3.6}$$

where $E_{tot}^{bcc}(\vec{\sigma})$ is the total energy of an alloy, c_p is the average concentration of the atom p, $E_{tot}^{bcc}(p)$ is the reference total energy of a pure atom p in the bcc lattice and $\vec{\sigma}$ is the vector of configurational variables.

3.2 Cluster Expansion model

The Cluster Expansion (CE) method can also be used to obtain the enthalpy of mixing values following the equation:

$$\Delta H^{bcc}_{mix_{CE}}(\vec{\sigma}) = \sum_{\omega} m_{\omega} J_{\omega} \langle \Gamma_{\omega'}(\vec{\sigma}) \rangle_{\omega} \tag{3.7}$$

where ω denotes clusters, the term m_{ω} represents the multiplicity factors, J_{ω} are effective cluster interactions derived from a set of DFT calculations applying the structure inversion approach and the term $\langle \Gamma_{\omega'}(\vec{\sigma}) \rangle$ stands for the average correlation functions. Cluster function can be described as follows:

$$\Gamma^{(s)}_{\omega,n}(\vec{\omega}) = \gamma_{j_1 K}(\sigma_1)\gamma_{j_2 K}(\sigma_2) \cdots \gamma_{j_{|\omega|} K}\left(\sigma_{|\omega|}\right) \tag{3.8}$$

where $(s) = (j_1, j_2 \ldots j_{|\omega|})$ denotes the pattern of assigning point functions to the cluster. Point functions $\gamma_{j,K}(\sigma_i)$ are then defined:

$$\gamma_{j,K}(\sigma_i) = \begin{cases} 1 & \text{if } j = 0 \\ -cos\left(2\pi \left\lceil \frac{j}{2} \right\rceil \frac{\sigma_i}{K}\right) & \text{if } j > 0 \text{ and odd} \\ -sin\left(2\pi \left\lceil \frac{j}{2} \right\rceil \frac{\sigma_i}{K}\right) & \text{if } j > 0 \text{ and even} \end{cases} \tag{3.9}$$

where $\sigma_i = (0,1,2 \ldots K-1)$ denotes the index of point function. The 2-body correlation functions are then defined as a product of pair probabilities in a following matter:

$$\left\langle \Gamma^{(s)}_{2,n} \right\rangle = \left\langle \Gamma^{ij}_{2,n} \right\rangle = \sum_{a=1}^{K} \sum_{b=1}^{K} \gamma_i(\sigma_a)\gamma_j(\sigma_b) y^{ab}_n \tag{3.10}$$

where y^{ab}_n represents the probability of locating two atoms, *a* and *b*, within a specific shell, indicated by the label *n*. The 3-body correlation functions can be defined in a similar manner as follows:

$$\left\langle \Gamma_{3,n}^{(s)} \right\rangle = \left\langle \Gamma_{3,n}^{ijk} \right\rangle = \sum_{a=1}^{K} \sum_{b=1}^{K} \sum_{c=1}^{K} \gamma_i(\sigma_a)\gamma_j(\sigma_b)\gamma_k(\sigma_c) y_n^{abc} \tag{3.11}$$

where y_n^{abc} represents the probability of locating three atoms, a, b and c, within a specific shell, indicated by the label n.

3.3 Monte Carlo simulations

Canonical Exchange Monte Carlo (CEMC) is a simulation method used in computational statistical mechanics to study systems at constant temperature and particle number. It is broadly used to investigate the phase transitions, structural changes and thermodynamic properties of a given alloy.

Within this work, the simulations were performed by creating a fully disordered random configuration at either 2000 K or 3000 K, depending on the size of the supercell, and then annealed in the so-called simulated annealing procedure, using different temperature steps, usually 10 K or 100 K. For each finite temperature, a series of exchanges involving neighboring atoms within the lattice was executed, and the resulted total energy of system was calculated. If, as a result of such exchange, the total energy has decreased, then the exchange of the atoms was accepted. In case the energy increased, the exchange was accepted with a probability defined as $e^{\left(-\frac{\Delta E}{k_B T}\right)}$. In the next step the energy is averaged across all exchanges, and the newly updated atomic configuration transitions to the simulations at a different temperature.

The Alloy Theoretic Automated Toolkit (ATAT) package developed by van de Walle, Asta and Ceder was used to carry out MC simulations withing this work.

3.3.1 Chemical short-range order parameter

In 1951 Warren and Cowley introduced the Warren-Cowley short-range order parameter as a metric used to describe the local atomic arrangements in disordered alloys. In a crystal, the long-range order refers to the repeating pattern of atoms that extends throughout the entire crystal. Short-range order, on the other hand, involves the local atomic arrangements or correlations that deviate from the ideal long-range order. These deviations are often observed in alloys, where different types of atoms occupy the same crystal lattice positions in a disordered manner. They defined the so-called SRO parameter as:

$$\alpha_n^{ij} = 1 - \frac{y_n^{ij}}{c_i c_j} \tag{3.12}$$

where y_n^{ij} is the probability of finding atom i in the n-th nearest neighborhood of atom j, and $c_i c_j$ are the concentrations of atoms i and j. For the bcc system, the average SRO parameter can be calculated as:

$$\alpha_{avg}^{ij} = \frac{8\alpha_1^{ij} + 6\alpha_2^{ij}}{14} \tag{3.13}$$

where α_1^{ij} and α_2^{ij} denote the first and second nearest neighbors.

3.3.2 Free energy calculations

The free energy of mixing is a concept in thermodynamics that describes the energetic aspects of combining different substances at the molecular level. When two or more substances are mixed together, whether they are gases, liquids, or solids, there is a change in the system's free energy. This change is characterized by the Gibbs free energy of mixing F_{mix}. It can be described as:

$$F_{mix} = H_{mix} - TS_{mix}, \tag{3.14}$$

where H_{mix} is the enthalpy of mixing of a given system, S_{mix} is the entropy of mixing (reflecting the disorder or randomness of that system) and T is the absolute temperature. The entropy of mixing can be separated into two parts – the entropy of a random configuration S_{rand} and the configurational entropy S_{conf}. Equation (3.11) can be then written as:

$$F_{mix} = H_{mix} - T\left(-k_B \sum_i c_i ln(c_i) - \int_0^T \frac{C_{conf}(T')}{T'} dT'\right),$$

where c_i is the concentration of atom i and C_{conf} is the configurational heat obtained from the thermodynamic integration method (TDI) in MC simulations:

$$C_{conf}(T) = \frac{\langle H_{mix}(T)^2 \rangle - \langle H_{mix}(T) \rangle^2}{T^2}.$$

4 Results

This thesis is mainly based on the following key publications, along with their supplementary materials:

1. D. Sobieraj, J. S. Wróbel, T. Rygier, K. J. Kurzydłowski, O. El Atwani, A. Devaraj, E. Martinez, D. Nguyen-Manh, Chemical short-range order in derivative Cr–Ta–Ti–V–W high entropy alloys from the first-principles thermodynamic study, Physical Chemistry Chemical Physics, 2020, 22, 23929-23951, DOI: 10.1039/D0CP03764H
2. O. El-Atwani. N. Li, A. Devaraj, J. K. S. Baldwin, M. M. Schneider, D. Sobieraj, J. S. Wróbel, D. Nguyen-Manh, S.A. Maloy, E. Martinez, Outstanding radiation resistance of tungsten-based high-entropy alloys. Science Advances 5, eaav2002 (2019), DOI: 10.1126/sciadv.aav2002
3. D. Sobieraj, J. S. Wróbel, M. R. Gilbert, A. Litnovsky, F. Klein, K. J. Kurzydłowski,, D. Nguyen-Manh, Composition Stability and Cr-Rich Phase Formation in W-Cr-Y and W-Cr-Ti Smart Alloys, 2021, Metals 11, no. 5: 743, DOI: 10.3390/met11050743
4. D. Sobieraj, J. S. Wróbel, M. R. Gilbert, K. J. Kurzydłowski, D. Nguyen-Manh, Co-segregation of Y and Zr in W-Cr-Y-Zr alloys: First-principles modeling at finite temperature and application to SMART materials, Journal of Alloys and Metallurgical Systems, Volume 2, 2023, 100011, ISSN 2949-9178, DOI: 10.1016/j.jalmes.2023.100011.

The following chapter includes some of the results already presented in the aforementioned publications with their concise description.

4.1 High-entropy alloys phase stability at 0 K

The DFT-based CE model has been created, containing 682 bcc structures within the Cr-Ta-Ti-V-W system. The CE mapping has been applied to the entire 5-component system simultaneously, as opposed to conducting separate mappings for each subsystem. Analysis of the enthalpies of mixing for all binary combinations in the database has been undertaken to assess the nature of interactions between atoms in various binary configurations. Enthalpy of mixing values close to 0 eV/atom suggest the potential creation of a disordered solid solution,

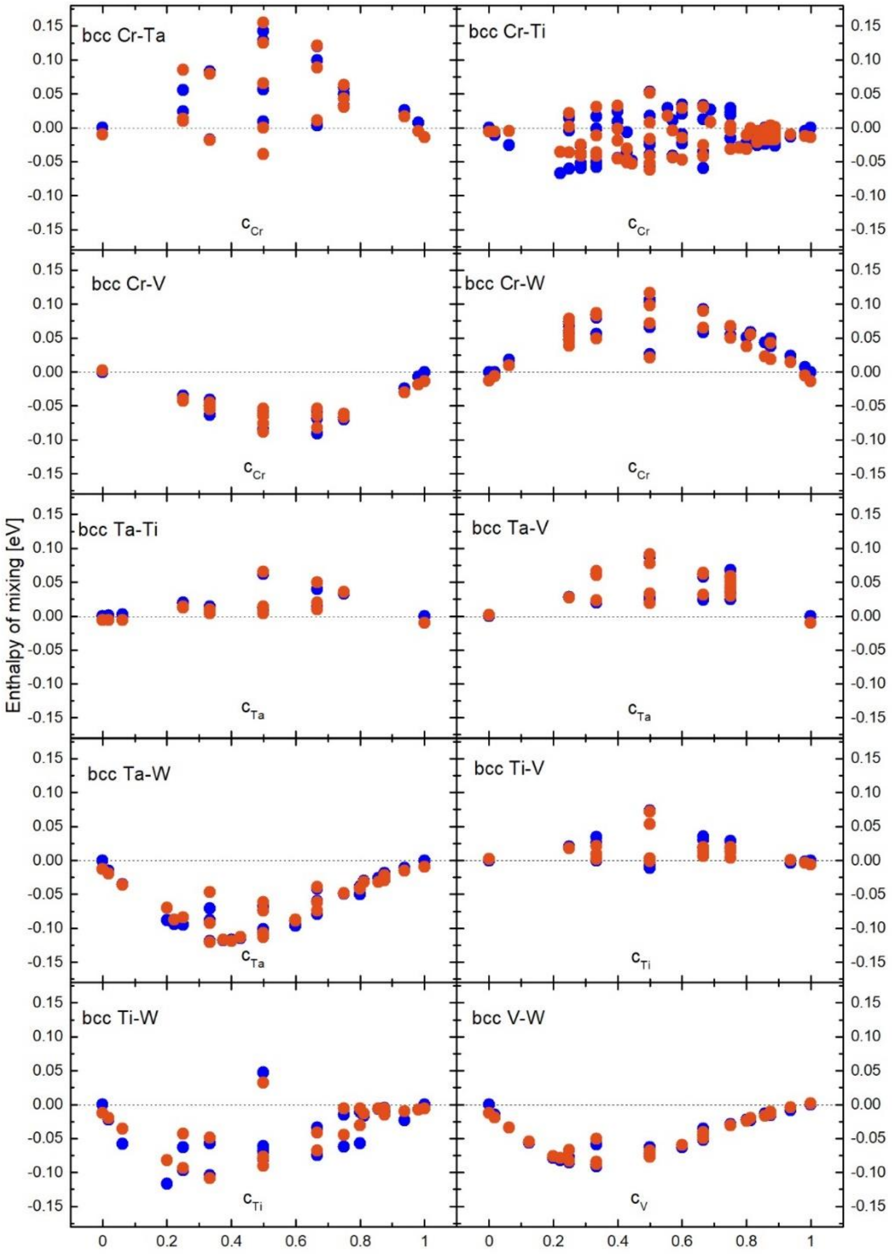

Figure 1 DFT (blue) and CE (red) enthalpies of mixing as a function of composition for all binary bcc structures included in the Cr-Ta-Ti-V-W model

negative values indicate a predisposition towards formation of the intermetallic phases, while positive values imply a tendency for atoms to segregate. The enthalpy of mixing outcomes for all binary alloys within the Cr-Ta-Ti-V-W systems are presented in Fig. 1 and in Appendix 1. In order to enhance the agreement between DFT and CE energies for the Cr-Ti system, additional structures for that binary were included, resulting in an improved overall agreement between DFT and CE results for the entire quinary Cr-Ta-Ti-V-W system. The cross-validation error between the DFT and CE methods was 10.2 meV/atom for the whole 5-component system.

Most of the structures in the Cr-Ta, Cr-W, Ta-Ti, Ta-V and Ti-V systems exhibit positive values of the enthalpy of mixing at absolute zero, which means that in most configurations atoms within those system tend to repel each other and segregate. On the opposite, most structures generated from the Cr-V, Ta-W, Ti-W and V-W systems have negative values of the enthalpy of mixing, suggesting tendency towards formation of clusters and ordering. Differences of the enthalpy of mixing values between the structures with the same compositions comes from different configurations of their unit cells. Usually, the structure with the lowest enthalpy of mixing at a given composition tends to be the most stable one, and a potential candidate for a ground-state.

One of the outcomes of the CE mapping into the DFT energies are effective cluster interactions, described in chapter 3.2. ECIs provide insight into the magnitude of the interactions between the atoms as a n-th neighbors. For the quinary Cr-Ta-Ti-V-W system interactions between pairs of atoms up to 4th nearest neighbor well included, as well as two smallest 3-body clusters.

4.2 High-entropy alloys phase stability and ordering at finite temperatures

Effective cluster interactions in the form of the CE Hamiltonian can be implemented into the MC simulations, which allows to investigate the temperature dependency of the enthalpy of mixing, short range order, and other thermodynamic properties of any given composition within the provided system. It is worth mentioning, that those simulations are not limited to the 5-component alloys, but allow investigating any other many-body combinations within that system, namely binary, ternary and quaternary alloys. ECIs values for the Cr-Ta-Ti-V-W system are given in the Appendix 1.

A 10x10x10 bcc cells have been used for the initial MC simulations, which resulted in 2000 atoms structures. Calculations were performed by generating a fully disordered atomic configuration at a stating temperature of 3000 K, and then performing a simulating quenching down to 100 K with a $\Delta T = 100$ K temperature step. At each temperature, 2000 accumulation and thermalization stages took place, which allowed to reach the equilibrium state.

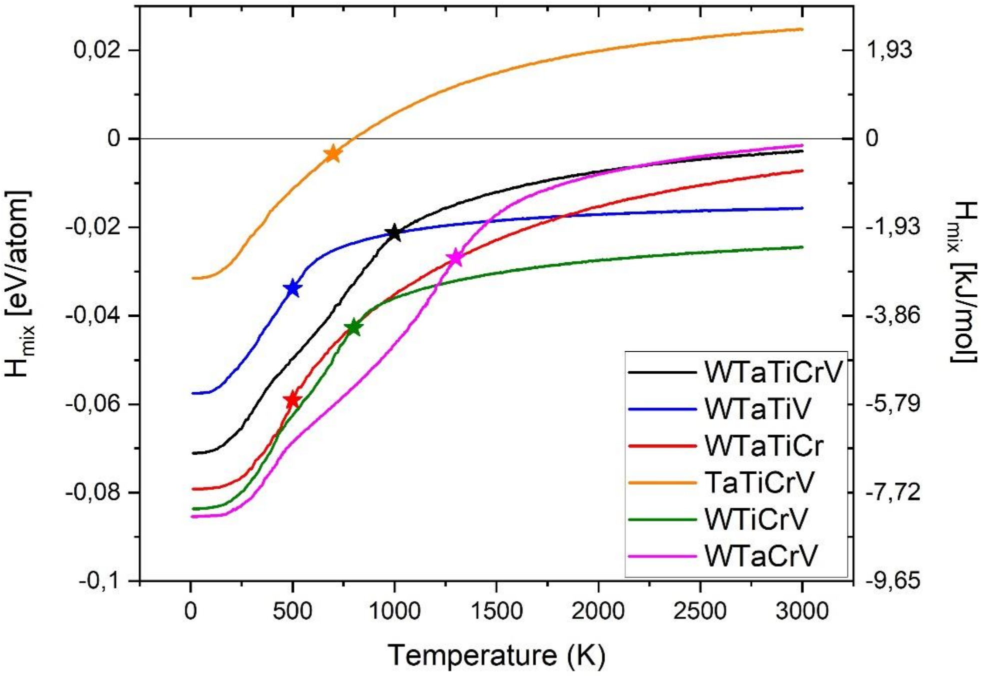

Figure 2 Enthalpy of mixing as a function of temperature for equiatomic quaternary and quinary alloys in the Cr-Ta-Ti-V-W system

To understand the underlying interactions between atoms in the Cr-Ta-Ti-V-W system, an equiatomic quinary, as well as 5 equiatomic quaternary alloys from 5 possible combinations of subsystems were analyzed. At Fig. 2 the enthalpy of mixing (H_{mix})

dependency on the temperature is shown. In addition to the H_{mix}, the order-disorder transition temperatures (*ODTT*) were computed, which allows to estimate at which temperature an alloy starts its transition towards the fully disordered state. The *ODTT* was defined as the highest inflection point on the enthalpy of mixing as a function of temperature plot, and is marked as stars in the Fig. 2. Additionally, specific values for analyzed equiatomic alloys are given in Table 1.

Table 1. Order-disorder transition temperature for equiatomic quaternary and quinary alloys

Composition	ODTT [K]
Cr-Ta-Ti-V-W	1000
Cr-Ta-Ti-W	500
Ta-Ti-V-W	500
Cr-Ta-V-W	1300
Cr-Ti-V-W	800
Cr-Ta-Ti-V	700

The Cr-Ta-Ti-W and Ta-Ti-V-W equiatomic alloys had the lowest *ODTT* among analyzed alloys – 500 K, followed by 700 K and 800 K for the Cr-Ta-Ti-V and Cr-Ti-V-W alloys, respectively. The quinary Cr-Ta-Ti-V-W alloy had second highest *ODTT* – 1000 K, while the highest value was observed for the quaternary Cr-Ta-V-W alloy – 1300 K. Above implies that alloys with either Cr or V removed are potentially reaching the disordered state at the lowest temperature among analyzed alloys.

To better understand the influence of pairs of atoms on the phase stability and *ODTT* of an alloy, the Warren-Cowley short-range order parameter as a function of temperature was computed. This parameter provides insight into the nature of interactions between atoms within defined pairs of elements – positive value of the SRO parameter indicates the tendency towards segregation of atoms, while negative values suggest a potential attraction between atoms, which results in clustering and ordering. By definition, a fully disordered alloy would have the SRO parameter values for all pairs equal to 0, without any tendencies towards repelling or attraction between atoms. In practice such cases do not exist, so the goal in creating a disordered alloy is to achieve the SRO parameter values as close to 0 as possible.

In Fig.3, the SRO parameter as a function of temperature is given for the equiatomic quinary Cr-Ta-Ti-V-W alloy and 5 sub-quaternary equiatomic alloys. For each composition, representative structures are shown at 400 K and 800 K. In quinary Cr-Ta-Ti-V-W alloy and quaternary Ta-Ti-V-W, Cr-Ta-V-W and Cr-Ta-Ti-W alloys, strongly negative SRO parameter

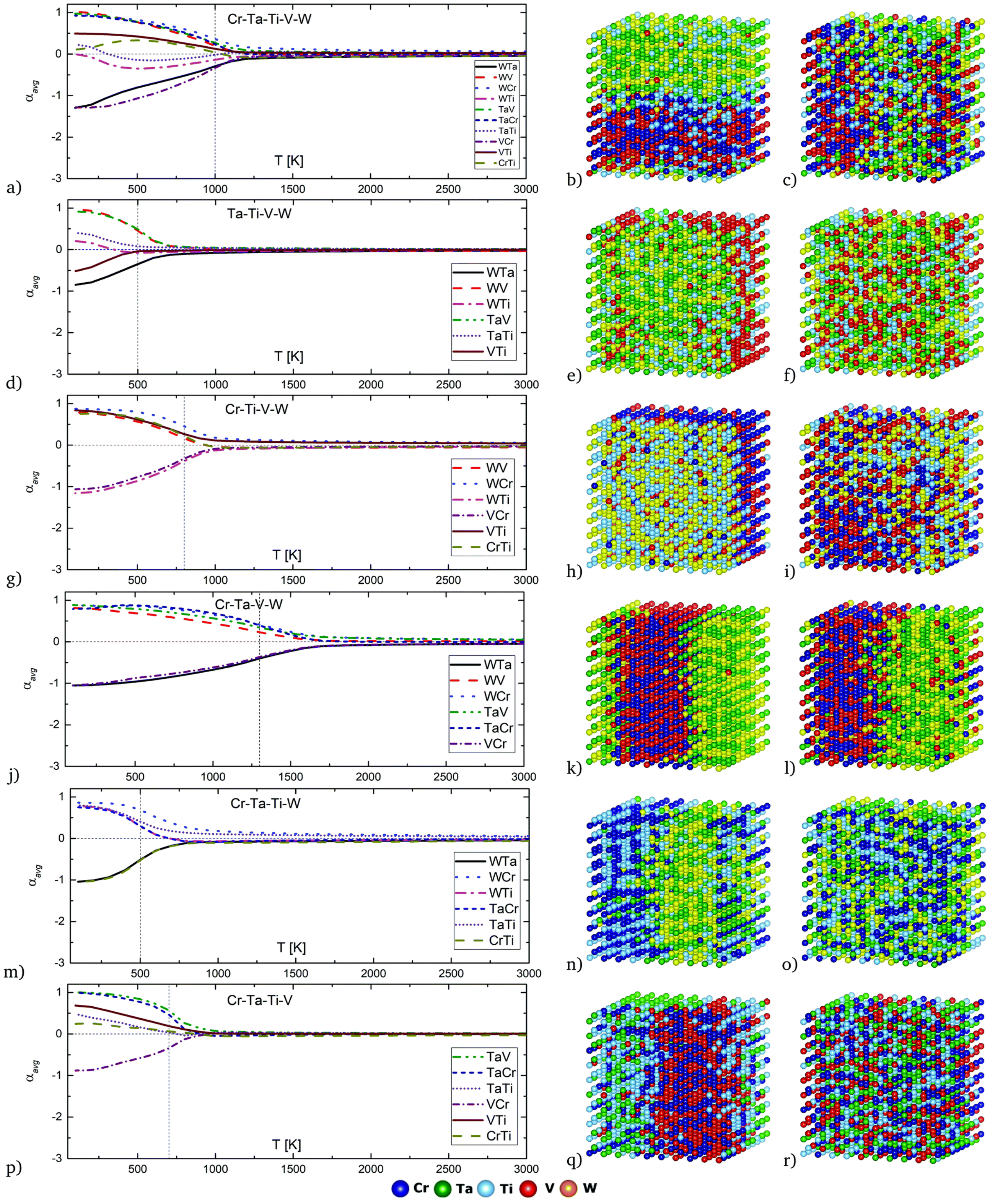

Figure 3 Average short-range order parameter as a function of temperature for quaternary and quinary alloys in the Cr-Ta-Ti-V-W system. Images b, e, h, k, n, q are representative structures generated at 400 K, images c, f, I, l, o, r are representative structure generated at 800 K.

value in the whole temperature range has been observed for Ta-W pair, indicating strong attraction between those atoms. Similarly, the Cr-V pair has shown the same tendency in Cr-Ta-Ti-V-W, Cr-Ti-V-W, Cr-Ta-V-W and Cr-Ta-Ti-V alloys. On the other hand, mostly positive values of the SRO parameter have been observed for Ta-V, Cr-Ti and Cr-W pairs, suggesting a tendency towards segregation between those atoms.

The vertical lines in Fig. 3 represent the *ODTT* calculated as the highest inflection point among all pairs present in the specific alloy. It has been found out, that the *ODTT* calculated from the SRO plots is in agreement with those calculated from the enthalpies of mixing and shown in Fig. 1. By comparing representative structures generated at 800 K, it has been observed that indeed the Cr-Ta-Ti-W and Ta-Ti-V-W alloys are reaching a disordered state at lower temperatures than for example Cr-T-V-W alloy, where clear separation between Cr-V and Ta-W clusters is still present.

The initial investigation of the atomic interactions in the equiatomic alloys led to a conclusion that in the alloys where these pairs are present, the Ta-W and Cr-V pairs exert the most significant influence on the onset of the *ODTT*. In order to better understand how singular element concentrations influence the *ODTT*, the calculations for pseudo-binary alloys were necessary. A series of MC simulations were performed for $A_x(BCDE)_{1-x}$ alloys (where $x = \{0;\ 0.05;\ 0.1; \dots; 0.75;\ 0.8; 0.85\}$). The idea was to create multiple pseudo-binary alloys with different concentrations of a single element from the Cr-Ta-Ti-V-W system, while the

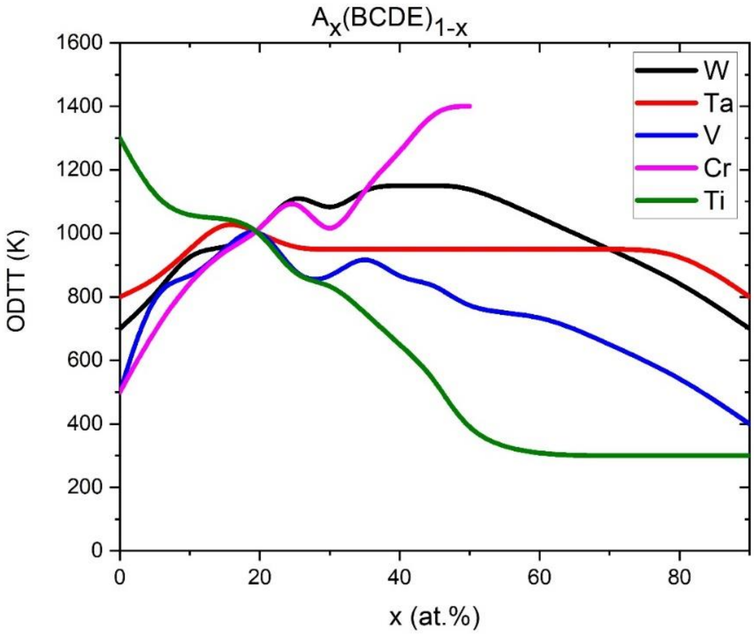

Figure 4 Order-disorder transition temperature as a function of element concentration. Remaining elements are kept at the equiatomic concentrations

remaining elements remained in the equiatomic ratio. In total, MC simulations for over 80 distinct pseudo-binary alloy composition have been performed. It has been observed that increasing the concentration of Cr in the system rapidly increased the *ODTT*, up to 1400 K observed for the $Cr_{0.5}(TaTiVW)_{0.5}$ alloy. Increasing the concentration of V from 0 to 20% increased the *ODTT* up to 1000 K, but further addition actually reduced the *ODTT* down to 400 K for the $V_{0.9}(CrTaTiW)_{0.1}$ alloy. Very strong influence on the lowering of the *ODTT* has been observed for Ti, which reduced the *ODTT* down to 300 K at around 50% Ti concentration. The behavior of Ti the Cr-Ta-Ti-V-W system can be explained by the fact that increasing the Ti concentration reduced the concentration of Cr-V and Ta-W pairs, which displayed a strong tendency towards ordering (between atoms) and segregation (between pairs of atoms).

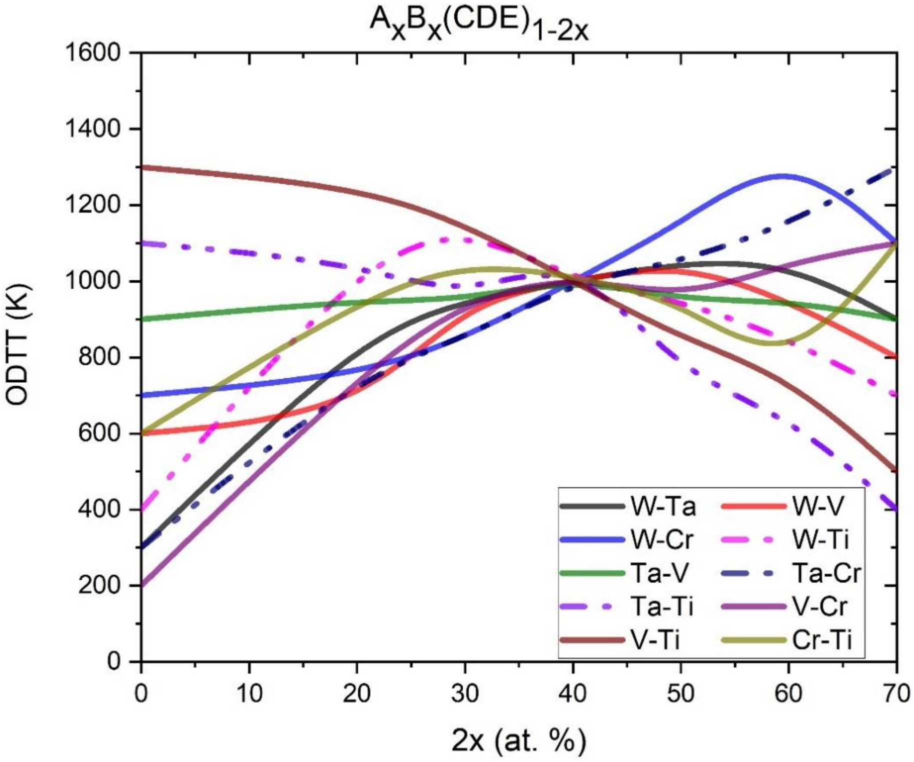

Figure 5 Order-disorder transition temperature as a function of pairs concentration. Remaining elements are kept at the equiatomic concentrations.

Recently, the W38-Ta36-Cr15-V11 alloy samples with outstanding radiation resistance have been sintered using the magnetron sputtering deposition system from pure metal targets. The developed CE model for the Cr-Ta-Ti-V-W binary system allowed to explain the presence of the Cr-V precipitates observed in annealed and irradiated samples. The local concentration profile of a 30x30x30 simulation cell (Fig. 6) has been compared to the Atom Probe Tomography (APT) local concentration profile of the sintered samples (Fig. 6b,d). Similar trend has been observed in both cases – the Cr and V concentration significantly increased inside the observed precipitates, while Ta and W atoms remained within the matrix. The outcomes of the analytical modelling. which illustrated the segregation of Cr-V–enriched precipitates from the Ta-W matrix, aligned with the characteristics seen in the APT analysis for the samples in their as-deposited state, as well as the examinations of thermal stability. Moreover, the modelling findings support observation of precipitates under irradiation, showing a significant thermodynamic driving force for the system to undergo the phase separation.

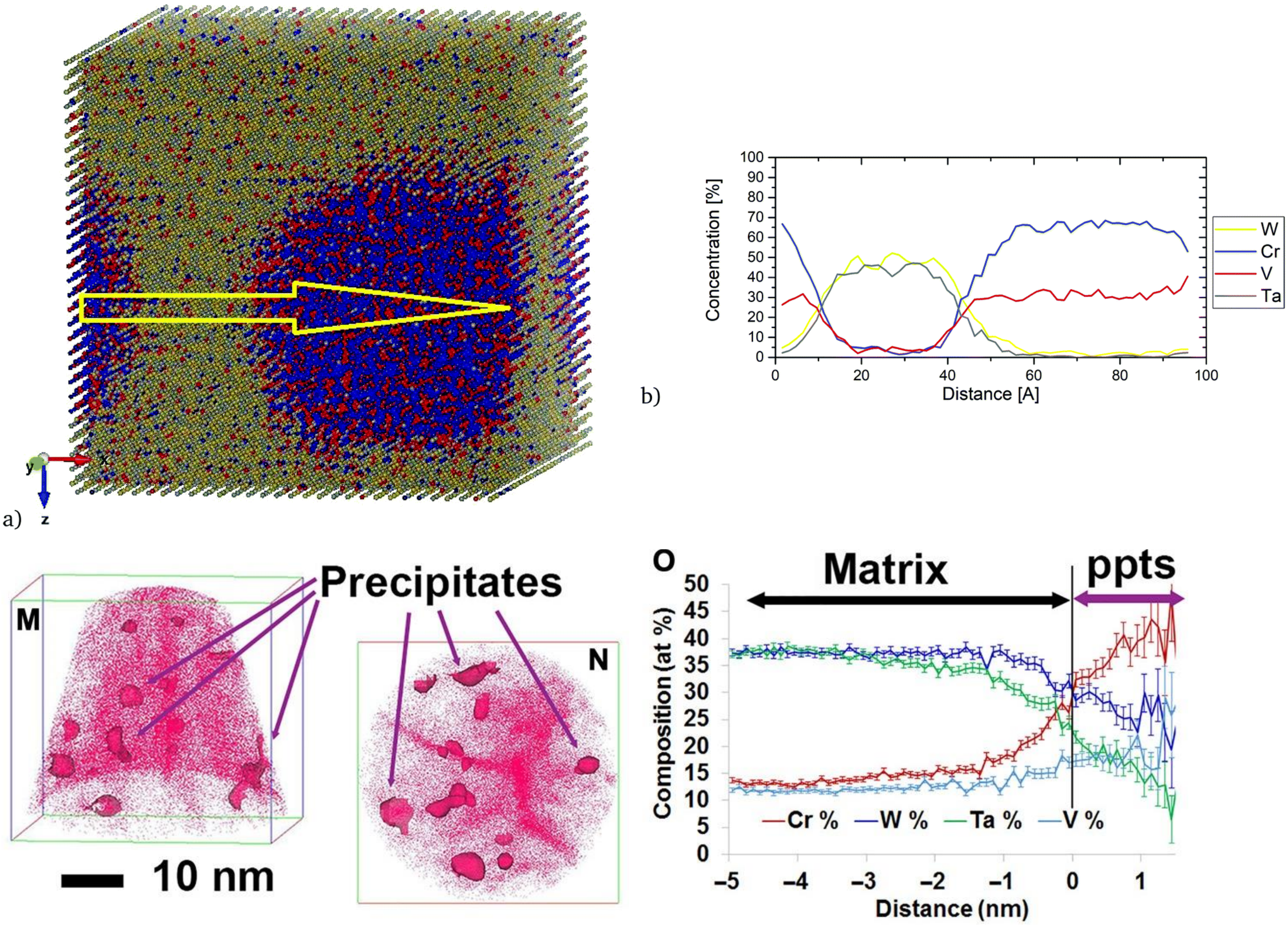

Fig. 6 Local concentration profile in the W38-Ta36-Cr15-V11 alloy at 1000 K, calculated from MC simulations, compared to the local concentration profile of the specimen sintered in the Los Alamos National Laboratory via magnetron sputtering.

In Fig. 7, the thermodynamic properties such as the enthalpy of mixing, free energy of mixing and entropy contribution to the free energy of mixing are given for the W38-Ta36-Cr15-V11 alloy. Additional, Fig. 8 compares the free energy of mixing of the aforementioned alloy to that of the equiatomic CrTaVW alloy. Above 1100 K, the free energy of mixing of the refractory W38-Ta36-Cr15-V11 alloy is 0,02 eV/atom higher than for the equiatomic composition, while being relatively similar at lower temperatures.

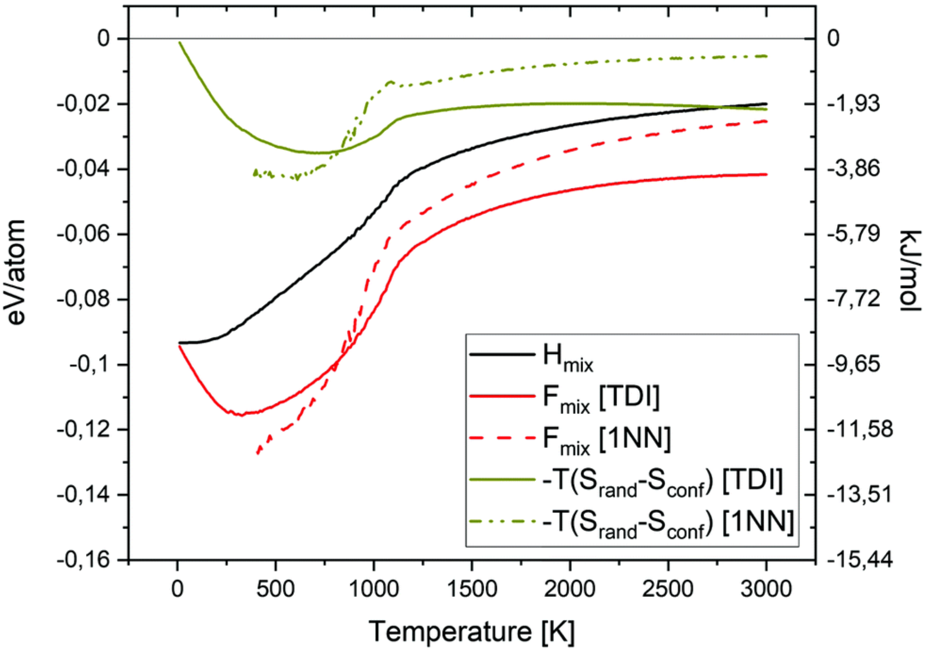

Fig. 7 Enthalpy of mixing, free energy of mixing and the entropy contribution to the free energy of mixing as a function of temperature for the W38-Ta36-Cr15-V11 alloy.

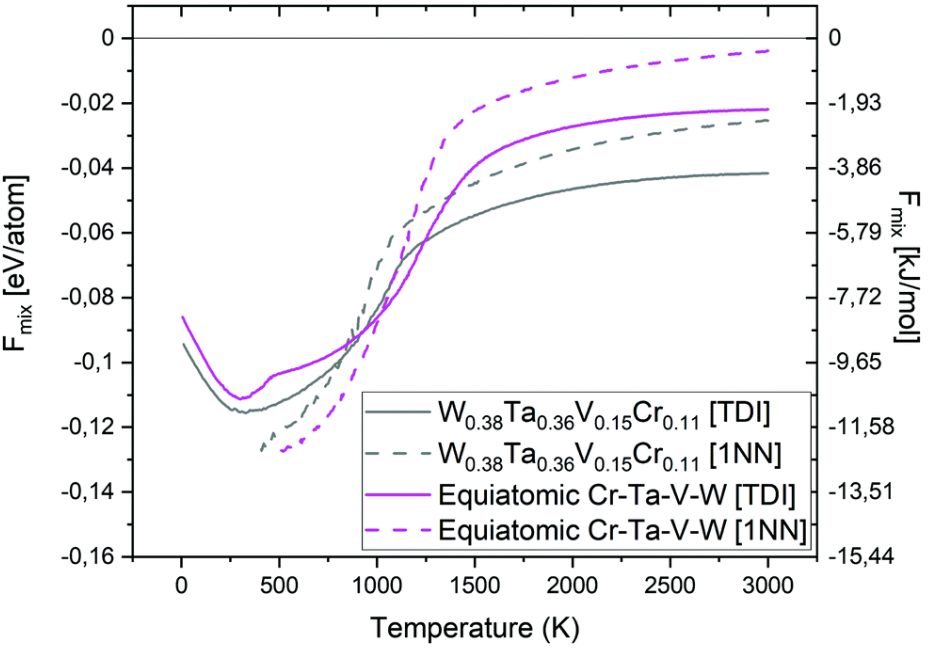

Fig. 8 Free energy of mixing as a function of temperature - a comparison between equiatomic CrTaVW alloy and W38-Ta36-V15-Cr11 alloy.

4.3 SMART materials phase stability at 0 K

Following the methodology used in HEAs, the DFT-based CE model has been developed for the Cr-Y-W ternary system, which was later extended to the quaternary with the addition of Zr. Initially, the phase stability of all binary subsystems at absolute zero has been analyzed (Fig. 9). All structures within Cr-Y, Cr-Zr, Cr-W, W-Y and W-Zr subsystems had positive values of the enthalpy of mixing, showing a potential tendency towards the atomic segregation. The only subsystem to contain structures with negative values of the enthalpy of mixing was Y-Zr – 20 out of 63 binary structures had H_{mix} values below 0. The cross-validation value between the DFT and CE methods for the quaternary Cr-Y-W-Zr system was 18.9 meV/atom.

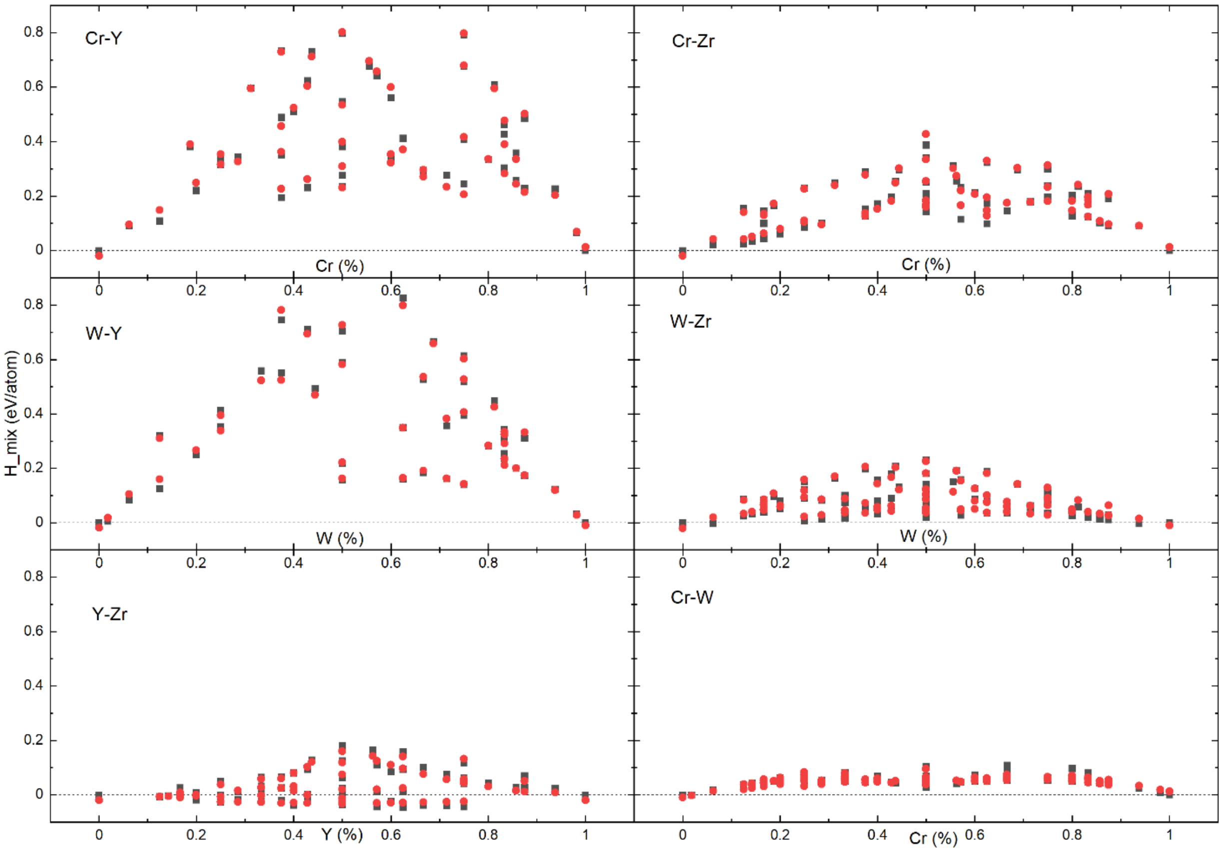

Fig. 9 DFT (blue) and CE (red) enthalpies of mixing as a function of composition for all binary bcc structures included in the Cr-W-Y-Zr model.

4.4 SMART materials phase stability and ordering at finite temperatures

Optimized effective cluster interactions for the Cr-W-Y-Zr system have been implemented in the MC simulations to determine the influence of the temperature and alloy composition on the phase stability and short-range ordering of SMART materials. Calculations have been performed for 10x10x10 bcc simulation cells for the reference $W_{70}Cr_{30}$ composition, as well as the $W_{70}Cr_{29}Y_1$ composition, which was earlier proven to be the optimum alloying components ratio for the stability of the protective Cr_2O_3 layer in plasma-facing components.

The formation of Y-rich precipitates has been observed even at elevated temperatures above 1800 K in the $W_{70}Cr_{29}Y_1$ alloy (Fig. 10d,e,f). The addition of Y also resulted in the shift of the ODTT transition from the 1700 K for the binary $W_{70}Cr_{30}$ composition to the 1300 K for the ternary $W_{70}Cr_{29}Y_1$ alloy. Maintaining higher ODTT in self-passivating plasma-facing components is beneficial due to the wider range of temperature at which the protective layer forms as a result of the spinodal decomposition. Therefore the addition of Y, while generally stabilizing the layer and increasing its oxidation resistance, reduced the temperature range at which the spinodal decomposition is present. To partially alleviate this issue, the addition of Zr

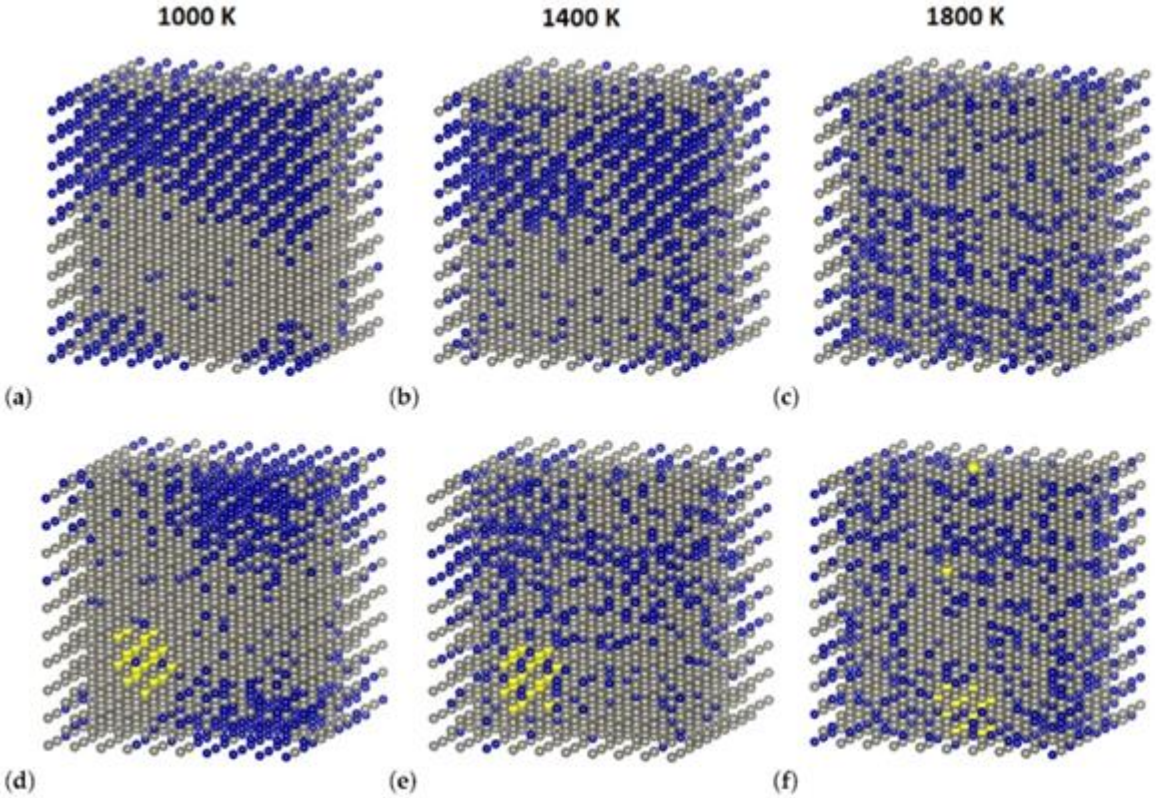

Fig. 10 Representative structures generated by MC simulations for a,b,c) W70Cr30 and d,e,f) W70Cr29Y1 alloys at 1000 K (left column), 1400 K (middle column) and 1800 K (right column).

to the system was proposed. In Fig.13 the average SRO parameter values as a function of temperature are given for the quaternary $W_{70}Cr_{28}Y_1Zr_1$ and $W_{70}Cr_{29}Y_{0.5}Zr_{0.5}$ are given. Strongly negative values of the SRO parameter in the whole temperature range have been observed for the Y-Zr pair – suggesting significant attraction between those elements. Remaining pairs of atoms have shown positive values of the SRO parameter, indicating tendency towards segregation.

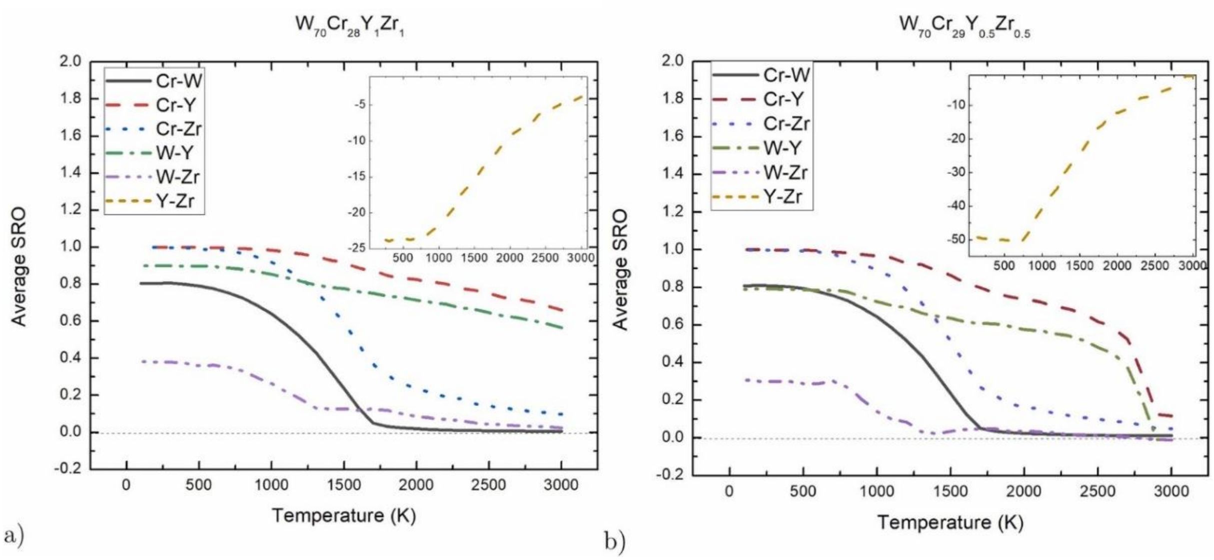

Fig. 13 Average short-range order as a function of temperature comparison between a) $W_{70}Cr_{28}Y_1Zr_1$ and b) $W_{70}Cr_{29}Y_{0.5}Zr_{0.5}$ alloys.

In Fig. 14 the representative structure images generated from MC for $W_{70}Cr_{28}Y_1Zr_1$ alloy at 300 K, 1000 K and 1800 K are given. Similarly, the representative structures for

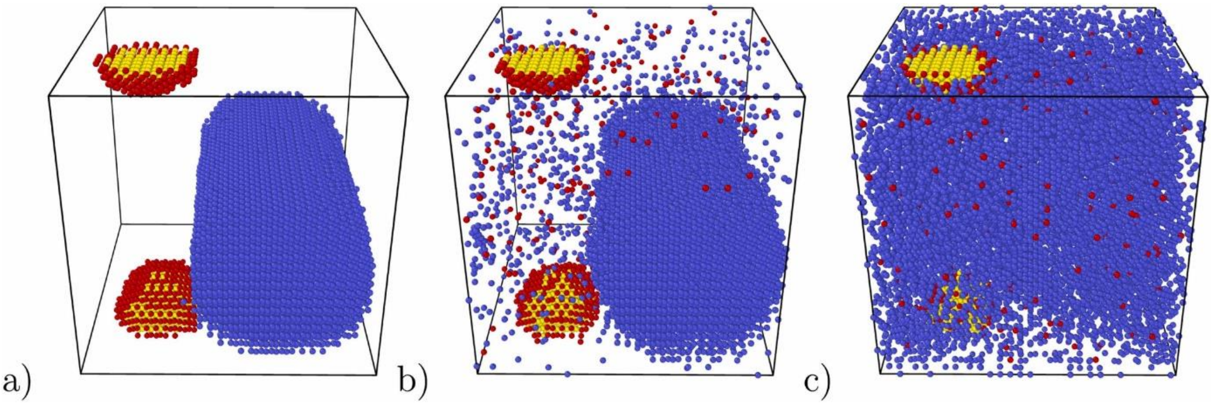

Figure 14 Representative structure images generated from MC of W70Cr28Y1Zr1 alloy at a) 300 K, b) 1000 K and c) 1800 K. Cr, Y and Zr are represented as blue, yellow and red atoms, respectively. W atoms are not shown for visual clarity.

$W_{70}Cr_{29}Y_{0.5}Zr_{0.5}$ alloy are given in Fig. 15. In both cases the formation of Y-Zr precipitation has been observed, even at elevated temperatures above 1800 K. Y atoms were present inside the precipitate, while Zr atoms completely surrounded the Y-rich cluster, separating it from the matrix of an alloy. Separation of the Cr from the W (removed from the images for clarity) has also been present at temperatures above 1000 K.

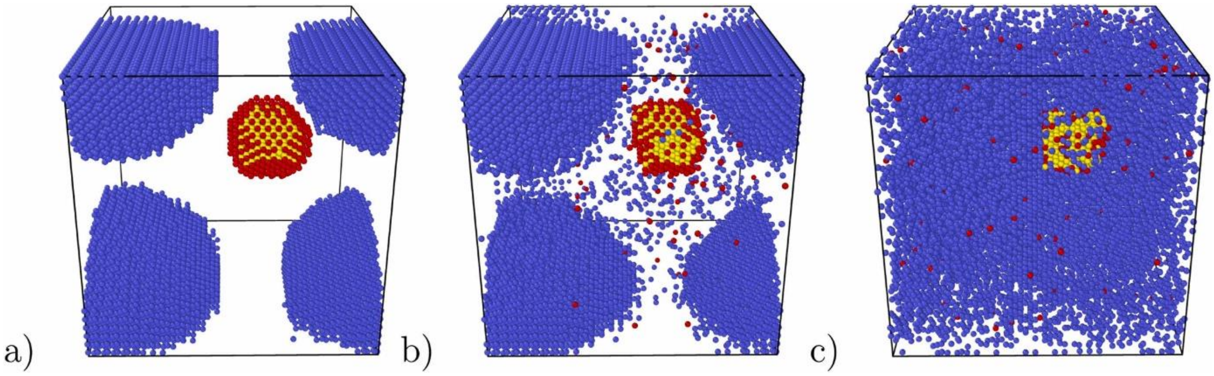

Fig. 15 Representative structure images generated from MC of $W_{70}Cr_{29}Y_{0.5}Zr_{0.5}$ alloy at a) 300 K, b) 1000 K and c) 1800 K. Cr, Y and Zr are represented as blue, yellow and red atoms, respectively. W atoms are not shown for visual clarity.

The addition of 1%at. of Zr resulted in the shift of the ODTT to 1500 K, value between those for ternary $W_{70}Cr_{29}Y_1$ (1300 K) and binary $W_{70}Cr_{30}$ (1700 K), proving to be desired compromise between the enhanced stability of the protective oxide layer while maintaining wider temperature range of the spinodal decomposition between Cr and W.

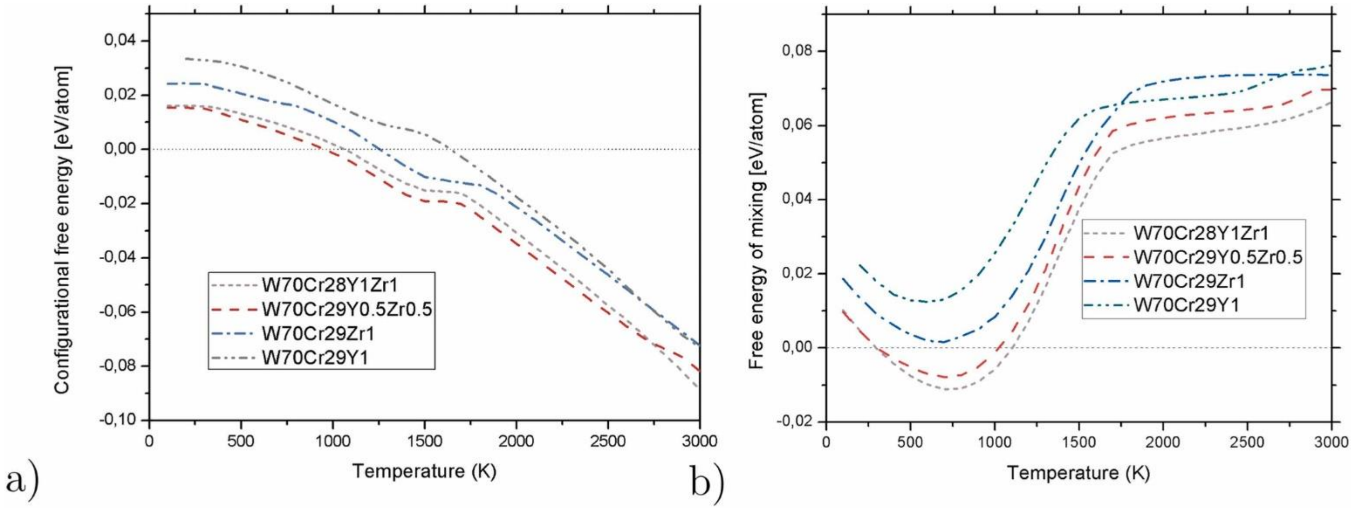

Fig. 16 Configurational free energy (a), and free energy of mixing (b) as a function of temperature for ternary $W_{70}Cr_{29}Y_1$ and $W_{70}Cr_{29}Y_1$ alloys, as well as quaternary $W_{70}Cr_{28}Y_1Zr_1$ and $W_{70}Cr_{29}Y_{0.5}Zr_{0.5}$ alloys.

5 Summary

- A DFT-based CE model, which includes the whole composition range, has been created for the quinary W-Cr-Ta-Ti-V system and quaternary W-Cr-Y-Zr system in bcc crystallographic lattice. Binary ground states reported in this work are in agreement with those available in literature.
- MC simulations based on the CE Hamiltonian have been performed to calculate temperature dependent properties of HEAs and SMART materials in a wide range of compositions.
- It has been shown that in HEAs from the W-Cr-Ta-Ti-V system, the strongest attraction occurs between Cr and V, as well as Ta and W atoms. The lowest order-disorder transition temperature (ODTT), therefore the widest range of temperatures at which disordered solid solution is present, has been observed for the quaternary W-Ta-Ti-V alloy.
- The model developed for the quinary W-Cr-Ta-Ti-V system has helped to explain the reasoning behind the formation of experimentally observed Cr and V-rich precipitates in the W38-Ta36-Cr15-V11 alloy with high radiation resistance.
- Calculations for the SMART materials revealed the existence of a co-segregation between Y and Zr in W-Cr-Y-Zr alloys. It has also been shown, that the addition of Y and Zr, even in small concentrations, has significant influence on the temperature of Cr-W spinodal phase decomposition in those alloys.
- The results of this study enable the optimization of chemical compositions and properties of materials for future plasma facing components.
- Obtained results confirm the hypothesis of this work, that the phase stability and short-range ordering of W-based high-entropy alloys in W-Cr-Ta-Ti-V system and SMART materials in W-Cr-Y-Zr system can be systematically predicted and optimized through first-principles modeling..

6 References

1 J. Knaster, A. Moeslang and T. Muroga, Materials research for fusion, Nat. Phys., 2016, 12, 424–434.

2 D. Stork and S. Zinkle, Introduction to the special issue on the technical status of materials for a fusion reactor, Nucl. Fusion, 2017, 57, 092001.

3 E. E. Bloom, The challenge of developing structural materials for fusion power systems, J. Nucl. Mater., 1988, 258–263, 7–17.

4 A. F. Rowcliffe, L. M. Garrison, Y. Yamamoto, L. Tan and Y. Katoh, Materials challenges for the fusion nuclear science facility, Fusion Eng. Des., 2018, 135, 290–301

6 R. G. Abernethy, Predicting the performance of tungsten in a fusion environment: a literature review, Mater. Sci. Technol., 2017, 33, 388–399.

7 T. Li, Y. Morgan, J. A. W. Van Dommellen, S. Anstusch, M. Reith, J. P. M. Hoefnagels, D. Terentyev, G. De Temmermman, K. Verbeken and D. G. M. Geers, Fracture behavior of tungsten-based composites exposed to steady-state/transient hydrogen plasma, Nucl. Fusion, 2020, 60, 046029.

8 B. Gludovatz, S. Wurster, A. Hoffmann and R. Pippan, Fracture toughness of polycrystalline tungsten alloys, Int. J. Ref. Met. and Hard Mater., 2010, 28, 674–678.

9 D. Rupp and S. M. Weygand, Anisotropic fracture behaviour and brittle-to-ductile transition of polycrystalline tungsten, Phil. Mag., 2010, 90, 4055.

10 O. El-Atwani, J. A. Hinks, G. Greaves, J. P. Allain and S. A. Maloy, Grain size threshold for enhanced irradiation resistance in nanocrystalline and ultrafine tungsten, Mater. Res. Lett., 2017, 5, 343–349.

11 O. El-Atwani, J. A. Hinks, G. Greaves, S. Gonderman, T. Qiu, M. Efe and J. P. Allain, In-situ TEM observation of the response of ultrafine- and nanocrystalline-grained tungsten to extreme irradiation environments. Sci. Rep., 2014, 4, 4716.

12 W. Dai, S. Liang, Y. Luo and Q. Yang, Int. J. Ref. Met. and Hard Mater., 2015, 50, 240–246.

13 A. Xu, C. Beck, D. E. J. Armstrong, K. Rajan, G. D. W. Smith, P. A. J. Bagot and S. G. Roberts, Ion-irradiation-induced clustering in W–Re and W–Re–Os alloys: A comparative study using atom probe tomography and nanoindentation measurements, Acta Mater., 2015, 87, 121–127.

14 M. Rieth, J. Reister, B. Dafferner and S. Baumgaetner, The Impact of Refractory Material Properties on the Helium Cooled Divertor Design, Fusion Sci. Technol., 2012, 61, 381–384.

15 S. Telu, A. Patra, M. Sankaranarayana, R. Mitra and S. K. Pabi, Microstructure and cyclic oxidation behavior of W–Cr alloys prepared by sintering of mechanically alloyed nanocrystalline powders, Int. J. Ref. Met. and Hard Mater., 2013, 36, 191–203.

16 D. Nguyen-Manh, M. Muzyk, M. Y. Lavrentiev and S. L. Dudarev, First-principles models for phase stability and radiation defects in structural materials for future fusion power-plant applications, J. Mater. Sci., 2012, 47, 7385–7398.

17 M. Muzyk, D. Nguyen-Manh, K. J. Kurzydłowski, N. L. Baluc and S. L. Dudarev, Phase stability, point defects, and elastic properties of WV and W-Ta alloys, Phys. Rev. B, 2011, 84, 104115.

18 M. Muzyk, D. Nguyen-Manh, J. Wróbel, K. J. Kurzydłowski, N. L. Baluc and S. L. Dudarev, First-principles model for phase stability, radiation defects and elastic properties of W–Ta and W–V alloys, J. Nucl. Mater., 2013, 442, S680–S683.

19 L. Romaner, C. Ambrosch-Draxl and R. Pippan, Effect of rhenium on the dislocation core structure in tungsten, Phys. Rev. Lett., 2010, 104, 195503.

20 Y. Ma, Q. F. Han, Z. Y. Zhou and Y. L. Liu, First-principles investigation on mechanical behaviors of W–Cr/Ti binary alloys, J. Nucl. Mater., 2016, 468, 105–112.

21 K. K. Arshad, W. Guo, J. Wang, M. Y. Zhao, Y. Yuan, Y. Zhang, B. Wang, Z. J. Zhou and G. H. Lu, Influence of vanadium precursor powder size on microstructures and properties of W–V alloy, Int. J. Ref. Met. and Hard Mater., 2013, 50, 59–64.

22 X. Hu, C. M. Parish, K. Wang, T. Koyanagi, B. P. Eftin and Y. Katoh, Transmutation-induced precipitation in tungsten irradiated with a mixed energy neutron spectrum, Acta Mater., 2019, 165, 51–61.

23 M. J. Lloyd, R. G. Abernethy, M. R. Gilbert, I. Griffiths, P. A. J. Bagot, D. Nguyen-Manh, M. P. Moody and D. E. J. Armstrong, Decoration of voids with rhenium and osmium transmutation products in neutron irradiated single crystal tungsten, Scripta Mater., 2019, 173, 96–100.

24 M. J. Lloyd, R. G. Abernethy, D. E. J. Armstrong, P. A. J. Bagot, M. P. Moody and D. Nguyen-Manh, Radiation-induced segregation in W-Re: from kinetic Monte Carlo simulations to atom probe tomography experiments, Eur. Phys. J. B, 2019, 92, 241.

25 C. H. Huang, L. Gharaee, Y. Zhao, P. Erhart and J. Marian, Mechanism of nucleation and incipient growth of Re clusters in irradiated W-Re alloys from kinetic Monte Carlo simulations, Phys. Rev. B, 2017, 96, 094108.

26 B. Cantor, I. T. H. Chang, P. Knight and A. J. B. Vincent, Microstructural development in equiatomic multicomponent alloys, Mater. Sci. and Eng. A, 2004, 375–377, 213–218.

27 J. W. Yeh, S. K. Chen, S. J. Lin, J. Y. Gan, T. S. Chin, T. T. Shun, C. H. Tsau and S. Y. Chang, Nanostructured high-entropy alloys with multiple principal elements: novel alloy design concepts and outcomes, Adv. Eng. Mat., 2004, 6, 299–303.

28 Y. Zhang, T. T. Zou, Z. Tang, M. C. Gao, K. A. Dahmen, P. K. Liaw and Z. P. Lu, Microstructures and properties of high-entropy alloys, Prog. Mater. Sci., 2014, 61, 1–93.

29 E. K. Pickering and N. G. Jones, High-entropy alloys: a critical assessment of their founding principles and future prospects, Int. Mater. Rev., 2016, 61, 183–202.

30 D. B. Miracle and O. N. Senkov, A critical review of high entropy alloys and related concepts, Acta Mater., 2017, 122, 448–511.

31 Z. Leong, J. S. Wróbel, S. L. Dudarev, R. Goodall, I. Todd and D. Nguyen-Manh, The effect of electronic structure on the phases present in high entropy alloys, Sci. Rep., 2017, 7, 39803.

32 M. Gao, D. B. Miracle, D. Maurice and X. Yan, High-entropy functional materials, J. Mater. Res., 2018, 33, 3138–3155.

33 E. P. George, W. A. Curtin and C. C. Tasan, High entropy alloys: A focused review of mechanical properties and deformation mechanisms, Acta Mater., 2020, 188, 435–474.

34 L. Lilensten, J. P. Couzinie, J. Bourgon, L. Perriere, D. Dirras, F. Prima and I. Guillot, Design and tensile properties of a bcc Ti-rich high-entropy alloy with transformation-induced plasticity, Mater. Res. Lett., 2017, 5, 110–116.

35 G. Dirras, L. Lilensten, P. Djemia, M. Laurent-Brocq, D. Tingaud, J. P. Couzinie, L. Perriere, T. Chauveau and I. Guillot, Elastic and plastic properties of as-cast equimolar TiHfZrTaNb high-entropy alloy, Mater. Sci. Eng. A, 2016, 654, 30–38.

36 O. N. Senkov, G. B. Wilks, J. M. Scott and D. B. Miracle, Mechanical properties of Nb25Mo25Ta25W25 and V20Nb20Mo20Ta20W20 refractory high entropy alloys, Intermetallics, 2011, 19, 698–706.

37 A. Fernandez-Caballero, M. Fedorov, J. S. Wróbel, P. M. Mummery and D. Nguyen-Manh, Configurational entropy in multicomponent alloys: Matrix formulation from ab initio based hamiltonian and application to the FCC Cr-Fe-Mn-Ni system, Entropy, 2019, 21, 68.

38 S. Gorsse, J. P. Couzinie and M. D. B., From high-entropy alloys to complex concentrated alloys, C. R. Physique, 2018, 19, 721–736.

39 D. Nguyen-Manh, V. Vitek and A. P. Horsfield, Environmental dependence of bonding: A challenge for modelling of intermetallics and fusion materials, Prog. Mater. Sci., 2007, 55, 255–298.

40 L. J. Santodonato, Y. Zhang, M. Feygenson, C. M. Parish, M. C. Gao, R. J. K. Weber, J. C. Neuefeind, Z. Tang and P. K. Liaw, Deviation from high-entropy configurations in the atomic distributions of a multi-principal-element alloy, Nat. Commun., 2015, 6, 5964.

41 J. S. Wróbel, D. Nguyen-Manh, M. Y. Lavrentiev, M. Muzyk and S. L. Dudarev, Phase stability of ternary fcc and bcc Fe-Cr-Ni alloys, Phys. Rev. B, 2015, 91, 024108.

42 A. Fernández-Caballero, J. S. Wróbel, P. M. Mummery and D. Nguyen-Manh, Short-range order in high entropy alloys: Theoretical formulation and application to Mo-Nb-Ta-VW system, J. Phase Equilibria Diffus., 2017, 38, 391–403.

43 O. El-Atwani, N. Li, M. Li, A. Devaraj, J. K. S. Baldwin, M. M. Schneider, D. Sobieraj, J. S. Wróbel, D. Nguyen-Manh, S. A. Maloy and E. Martinez, Outstanding radiation resistance of tungsten-based high-entropy alloys, Sci. Adv., 2019, 5, eaav2002.

44 Q. J. Li, H. Sheng and E. Ma, Strengthening in multi-principal element alloys with local-chemical-order roughened dislocation pathways, Nat. Commun., 2019, 10, 3563.

45 M. Fedorov, J. S. Wróbel, A. Fernadez-Caballero, K. J. Kurzydłowski and D. Nguyen-Manh, Phase stability and magnetic properties in fcc Fe-Cr-Mn-Ni alloys from first-principles modelling, Phys. Rev. B, 2020, 101, 174416.

46 S. N. Khan, J. B. Staunton and G. M. Stocks, Statistical physics of multicomponent alloys using KKR-CPA, Phys. Rev. B, 2016, 93, 054206.

47 P. Singh, A. V. Smirnov and D. D. Johnson, Ordering Transformations in High-Entropy Alloys, Phys. Rev. B, 2016, 91, 224204.

48 K. Jin, B. C. Sales, G. D. Stocks, G. M. Samolyuk, M. Daene, W. J. Weber, Y. Zhang and H. Bei, Tailoring the physical properties of Ni-based single-phase equiatomic alloys by modifying the chemical complexity, Sci. Rep., 2016, 6, 20159.

49 D. B. Miracle, G. B. Wilks, A. G. Dahlman and J. E. Dahlman, The strength of chemical bonds in solids and liquids, Acta Mater., 2011, 59, 7840–7854